Research Article | Vol. 26, No. 3 | 5 Feb 2018 | OPTICS EXPRESS 3489
Optics EXPRESS

Plasmon-enhanced fluorescence of submonolayer porphyrins by silver-polymer core-shell nanoparticles

JIA-XIN NIU,[1,3] CHENG-DA PAN,[1,3] YI-TING LIU,[1] SHI-TAO LOU,[1] E WU,[1,2] BO-TAO WU,[1,4] XIAO-LEI ZHANG,[1,2,5] AND QING-YUAN JIN[1,2,6]

[1]*State Key Laboratory of Precision Spectroscopy, East China Normal University, Shanghai 200062, China*
[2]*Collaborative Innovation Center of Extreme Optics, Shanxi University, Taiyuan, Shanxi 030006, China*
[3]*These authors contributed equally*
[4]*btwu@phy.ecnu.edu.cn*
[5]*xlzhang@admin.ecnu.edu.cn*
[6]*qyjin@phy.ecnu.edu.cn*

Abstract: We investigate the fluorescence from submonolayer porphyrin molecules near silver-polymer core-shell nanoparticles (NPs) at a well-controlled separation distance of about 1 nm – 5 nm. When porphyrin molecules are deposited on silver NPs with the plasmonic resonance peak at about 410 nm, which matches very closely with the 405-nm excitation laser and the absorption band of porphyrin molecules, their emission intensity is found to be enhanced due to the plasmonic resonant excitation enhancement, and shows a decline as the increasing polymer shell thickness. Meanwhile, the lifetime results demonstrate that there exists the fluorescence quenching due to the charge transfer and nonradiative energy transfer losses, which is also the main reason that the maximum enhancement factor obtained in experiment is only about 2.3, although the theoretical one is above 60 according to the electric field distribution near silver NPs calculated by finite-difference time-domain method.

OCIS codes: (240.6680) Surface plasmons; (250.5230) Photoluminescence; (160.4236) Nanomaterials.

References and links

1. X. S. Xie and R. C. Dunn, "Probing single molecule dynamics," Science **265**(5170), 361–364 (1994).
2. P. Avouris and B. N. J. Persson, "Excited states at metal surfaces and their non-radiative relaxation," J. Phys. Chem. **88**(5), 837–848 (1984).
3. E. Dulkeith, A. C. Morteani, T. Niedereichholz, T. A. Klar, J. Feldmann, S. A. Levi, F. C. J. M. van Veggel, D. N. Reinhoudt, M. Möller, and D. I. Gittins, "Fluorescence quenching of dye molecules near gold nanoparticles: radiative and nonradiative effects," Phys. Rev. Lett. **89**(20), 203002 (2002).
4. W. Gebauer, A. Langner, M. Schneider, M. Sokolowski, and E. Umbach, "Luminescence quenching of ordered π-conjugated molecules near a metal surface: Quaterthiophene and PTCDA on Ag(111)," Phys. Rev. B **69**(15), 155431 (2004).
5. P. Anger, P. Bharadwaj, and L. Novotny, "Enhancement and quenching of single-molecule fluorescence," Phys. Rev. Lett. **96**(11), 113002 (2006).
6. A. Kinkhabwala, Z. Yu, S. Fan, Y. Avlasevich, K. Müllen, and W. E. Moerner, "Large single-molecule fluorescence enhancements produced by a bowtie nanoantenna," Nat. Photonics **3**(11), 654–657 (2009).
7. K. T. Shimizu, W. K. Woo, B. R. Fisher, H. J. Eisler, and M. G. Bawendi, "Surface-enhanced emission from single semiconductor nanocrystals," Phys. Rev. Lett. **89**(11), 117401 (2002).
8. S. Kühn, U. Håkanson, L. Rogobete, and V. Sandoghdar, "Enhancement of single-molecule fluorescence using a gold nanoparticle as an optical nanoantenna," Phys. Rev. Lett. **97**(1), 017402 (2006).
9. Y. Chen, K. Munechika, and D. S. Ginger, "Dependence of Fluorescence Intensity on the Spectral Overlap between Fluorophores and Plasmon Resonant Single Silver Nanoparticles," Nano Lett. **7**(3), 690–696 (2007).
10. F. Tam, G. P. Goodrich, B. R. Johnson, and N. J. Halas, "Plasmonic enhancement of molecular fluorescence," Nano Lett. **7**(2), 496–501 (2007).
11. A. M. Kern and O. J. F. Martin, "Excitation and reemission of molecules near realistic plasmonic nanostructures," Nano Lett. **11**(2), 482–487 (2011).
12. S. W. Verbruggen, M. Keulemans, M. Filippousi, D. Flahaut, G. V. Tendeloo, S. Lacombe, J. A. Martens, and S. Lenaerts, "Plasmonic gold–silver alloy on TiO_2 photocatalysts with tunable visible light activity," Appl. Catal. B **156–157**, 116–121 (2014).

#318828 https://doi.org/10.1364/OE.26.003489
Journal © 2018 Received 2 Jan 2018; revised 25 Jan 2018; accepted 29 Jan 2018; published 31 Jan 2018

Optics EXPRESS

13. S. W. Verbruggen, M. Keulemans, J. A. Martens, and S. Lenaerts, "Predicting the Surface Plasmon Resonance Wavelength of Gold–Silver Alloy Nanoparticles," J. Phys. Chem. C **117**(37), 19142–19145 (2013).
14. D. Conklin, S. Nanayakkara, T. H. Park, M. F. Lagadec, J. T. Stecher, X. Chen, M. J. Therien, and D. A. Bonnell, "Exploiting plasmon-induced hot electrons in molecular electronic devices," ACS Nano **7**(5), 4479–4486 (2013).
15. P. Banerjee, D. Conklin, S. Nanayakkara, T. H. Park, M. J. Therien, and D. A. Bonnell, "Plasmon-induced electrical conduction in molecular devices," ACS Nano **4**(2), 1019–1025 (2010).
16. M. C. Chen, Y. L. Yang, S. W. Chen, J. H. Li, M. Aklilu, and Y. Tai, "Self-assembled monolayer immobilized gold nanoparticles for plasmonic effects in small molecule organic photovoltaic," ACS Appl. Mater. Interfaces **5**(3), 511–517 (2013).
17. T. Fukuura, "Plasmons excited in a large dense silver nanoparticle layer enhancethe luminescence intensity of organic light emitting diodes," Appl. Surf. Sci. **346**, 451–457 (2015).
18. P. K. Jain, X. Huang, I. H. El-Sayed, and M. A. El-Sayed, "Noble Metals on the Nanoscale: Optical and Photothermal Properties and Some Applications in Imaging, Sensing, Biology, and Medicine," Acc. Chem. Res. **41**(12), 1578–1586 (2008).
19. S. Lal, S. Link, and N. J. Halas, "Nano-optics from sensing to waveguiding," Nat. Photonics **1**(11), 641–648 (2007).
20. H. Yu, Y. Luo, K. Beverly, J. F. Stoddart, H. R. Tseng, and J. R. Heath, "The molecule-electrode interface in single-molecule transistors," Angew. Chem. Int. Ed. Engl. **42**(46), 5706–5711 (2003).
21. D. K. James and J. M. Tour, "Electrical Measurements in Molecular Electronics," Chem. Mater. **16**(23), 4423–4435 (2004).
22. Y. Xue, C. Ding, Y. Rong, Q. Ma, C. Pan, E. Wu, B. Wu, and H. Zeng, "Tuning Plasmonic Enhancement of Single Nanocrystal Upconversion Luminescence by Varying Gold Nanorod Diameter," Small **13**(36), 1701155 (2017).
23. R. Bonnett, "Photosensitizers of the porphyrin and phthalocyanine series for photodynamic therapy," Chem. Soc. Rev. **26**(1), 19–33 (1995).
24. Z. C. Dong, X. L. Guo, A. S. Trifonov, P. S. Dorozhkin, K. Miki, K. Kimura, S. Yokoyama, and S. Mashiko, "Vibrationally resolved fluorescence from organic molecules near metal surfaces in a scanning tunneling microscope," Phys. Rev. Lett. **92**(8), 086801 (2004).
25. Y. Wakayama, J. P. Hill, and K. Ariga, "Real-time STM observation of molecular dynamics on a metal surface," Surf. Sci. **601**(18), 3984–3987 (2007).
26. Z. C. Dong, X. L. Zhang, H. Y. Gao, Y. Luo, C. Zhang, L. G. Chen, R. Zhang, X. Tao, Y. Zhang, J. L. Yang, and J. G. Hou, "Generation of molecular hot electroluminescence by resonant nanocavity plasmons," Nat. Photonics **4**(1), 50–54 (2010).
27. N. G. Bastús, F. Merkoçi, J. Piella, and V. Puntes, "Synthesis of Highly Monodisperse Citrate-Stabilized Silver Nanoparticles of up to 200 nm: Kinetic Control and Catalytic Properties," Chem. Mater. **26**(9), 2836–2846 (2014).
28. R. Asapu, N. Claes, S. Bals, S. Denys, C. Detavernier, S. Lenaerts, and S. W. Verbruggen, "Silver-polymer core-shell nanoparticles for ultrastable plasmon-enhanced photocatalysis," Appl. Catal. B **200**, 31–38 (2017).
29. D. W. Lynch and W. R. Hunter, "Silver (Ag)," in Handbook of Optical Constants of Solids, E. D. Palik, ed. (Academic, 1985).
30. L. Moroni, C. Gellini, P. R. Salvi, A. Marcelli, and P. Foggi, "Excited states of Porphyrin Macrocycles," J. Phys. Chem. A **112**(44), 11044–11051 (2008).
31. S. Berner, M. Brunner, L. Ramoino, H. Suzuki, H. J. Güntherodt, and T. A. Jung, "Time evolution analysis of a 2D solid-gas equilibrium: a model system for molecular adsorption and diffusion," Chem. Phys. Lett. **348**(3-4), 175–181 (2001).
32. S. Suto, W. Uchida, M. Yashima, and T. Goto, "Luminescence quenching of an ultrathin tetraphenylporphyrin film on a conductive SnO_2 substrate," Phys. Rev. B Condens. Matter **35**(9), 4393–4397 (1987).
33. S. Hamai, N. Tamai, and H. Masuhata, "Excimer Formation of Pyrene in a Solid/Polymer Solution Interface Layer. A Time-Resolved Total Internal Reflection Fluorescence Study," J. Phys. Chem. **99**(14), 4980–4985 (1995).
34. X. L. Zhang, L. G. Chen, P. Lv, H. Y. Gao, S. J. Wei, Z. C. Dong, and J. G. Hou, "Fluorescence decay of quasimonolayered porphyrins near a metal surface separated by short-chain alkanethiols," Appl. Phys. Lett. **92**(22), 223118 (2008).
35. P. Reineck, D. Gómez, S. H. Ng, M. Karg, T. Bell, P. Mulvaney, and U. Bach, "Distance and wavelength dependent quenching of molecular fluorescence by $Au@SiO_2$ core-shell nanoparticles," ACS Nano **7**(8), 6636–6648 (2013).

1. Introduction

Charge and energy transfer between optical molecules and nearby metals usually lead to fluorescence quenching [1–4]. In the meantime, however, metallic nanoparticles (NPs) have been well known to enhance the luminescence of molecules placed closely to the NPs [5–7]. The contradiction originates from the competition of damped molecular dipole oscillations or

Optics EXPRESS

orbital hybridization by interface interaction [3–5,8] and the highly concentrated incident field by the excited local plasmon resonances [9–11]. In the past several decades, a wealth of research has been done to study the amplification and inhibition of the fluorophores emission in the near field of metallic NPs [5,8]. Controlled molecular radiative properties by tuning the characteristics of NPs and molecule-NPs distances are of great importance [12,13] to understand the fundamental physics of plasmonic effects and benefit for the technological development of the measurement devices based on molecular fluorescence [14–16], such as organic light emitting diodes (OLEDs) [17], optical sensors [18, 19] and molecular electronic devices [20,21].

In spite of intense research on the plasmon-assisted fluorescence, however, it is still too complicated to fully understand the interplay between the plasmonic resonance of metallic NPs and the intrinsic optical properties of molecules in the several nanometers separation. Further studies are necessary to clarify the joint influence of the plasmonic resonance, the incident field, the molecular absorption and emission.

In our previous work, surface plasmon resonance wavelengths and NPs sizes could be well controlled to obtain the single nanocrystal upconversion luminescence enhancement [22]. Porphyrin molecules were chosen here as emitters because of their famous wide range of optical related applications [23,24] by constructing functional structures as building blocks [25]. And the emission properties of tetraphenyl porphyrin (TPP) molecules have been demonstrated to be affected dramatically by the localized plasmon mode [26]. In this work, the photoluminescence (PL) spectra and fluorescent lifetimes of submonolayer TPP molecules in the vicinity of the silver NPs strengthen the evidence of a plasmon-enhancement dominance over nonradiative decay at short distances (1 nm – 5 nm), when the resonant absorption and excitation are enhanced in the local near field.

2. Method

2.1 Silver-polymer core-shell nanoparticles fabrication

Ag NPs were prepared following the procedure described by Bastús group [27]. Resultant Ag NPs were synthesized by multi-growth step using silver seeds of 15 nm in diameter, which were synthesized as the following process. 1 mL of $AgNO_3$ (25 mM) was injected into a 20 mL aqueous solution containing sodium citrate (5 mM) and tannic acid (0.1 mM) after boiling, and the solution became bright yellow immediately. After 15 min, Ag seeds of about 15 nm were obtained. Then, the seed solution was diluted by adding 3.3 mL of Milli-Qwater instead of 3.9 mL seed solution in the same vessel. While the temperature of the solution was controlled to 90 °C, 0.5 mL of sodium citrate (25 mM), 1.5 mL of tannic acid (2.5 mM), and 1mL of $AgNO_3$ was sequentially injected with the time delay ~1 min and the solution was boiling for 30 min. After repeating the above process 13 times, the resultant size of Ag NPs was increased to 71.3 ± 6.8nm. Finally, the solution was purified by centrifugation (5000rpm, 20min) and dispersed in Milli-Qwater.

The synthesis of silver-polymer core-shell nanoparticles was based on the layer-by-layer (LBL) method [28]. The aqueous solutions of positively charged polyelectrolytes polyallyamine hydrochloride (PAH, 1 mM, Mw = 17500 g/mol) and negatively charged poly (styrene sulfonate) sodium salt (PSS, 0.5 mM, Mw = 70000 g/mol) were used. 15 ml PAH solution was dropwise added into 15 mL of the silver colloidal solution under vigorous stirring for 30 min in dark. Resultant Ag NPs capped PAH were rinsed three more times by Milli-Qwater to remove the excess PAH and then 5 ml solution was extracted for further characterization. Similarly, PSS layer was coated by mixing 10 ml PSS with 10 ml PAH-coated Ag NPs solution in the same process. The procedure was repeated to obtain multiple polymer layers. The size distribution of Ag NPs and the Ag NP-polymer core-shell structure were characterized by Transmission Electron Microscope (TEM).

Optics EXPRESS

2.2 Submonolayer porphyrins preparation

TPP submonolayer was thermally sublimated to gold or glass substrate in ~10^{-6} Pa vacuum at room temperature. The evaporation rate and the molecular coverage were controlled by constant heating voltage and current, then calibrated by scanning tunneling microscope (STM) images. The distribution of submonolayer porphyrins on substrates are characterized by STM and atomic force microscope (AFM).

2.3 Photoluminescence

The PL spectra and fluorescence lifetimes were obtained in vacuum at room temperature. A liquid nitrogen cooled charge coupled device (CCD) spectrometer (Princeton Instruments) was used to detect the steady-state PL spectra while a microchannel plate photomultiplier tube (Hamamatsu) combined with time-correlated single photon counting technique (Edinburgh Instruments) was used for photon counting and lifetimes measurements. A pulse picosecond diode laser at 405 nm (Edinburgh Photonics) was used to excite the samples.

2.4 Simulations

The numerical simulation was performed using the finite difference time domain (FDTD) method with the software FDTD Solutions (Lumerical Solution, Inc. Canada). Ag nanospheres with the diameter 71 nm and different shell thickness are placed on glass substrates. The dielectric constant of silver is taken from [29]. The refractive index of the surrounding matrix is set to be 1. A plane wave total field-scattered field source ranging from 300 to 600 nm is utilized as the incident light. The electric field distribution near Ag core-shell nanosphere is evaluated using the frequency domain field profile monitors. A three-dimensional nonuniform meshing is used, and a grid size of 0.5 nm is chosen for the inside and vicinity of Ag core-shell nanosphere. We use perfectly matched layer absorption boundary conditions as well as symmetric boundary conditions to reduce the memory requirement and computational time. The numerical results pass prior convergence testing.

3. Results and discussion

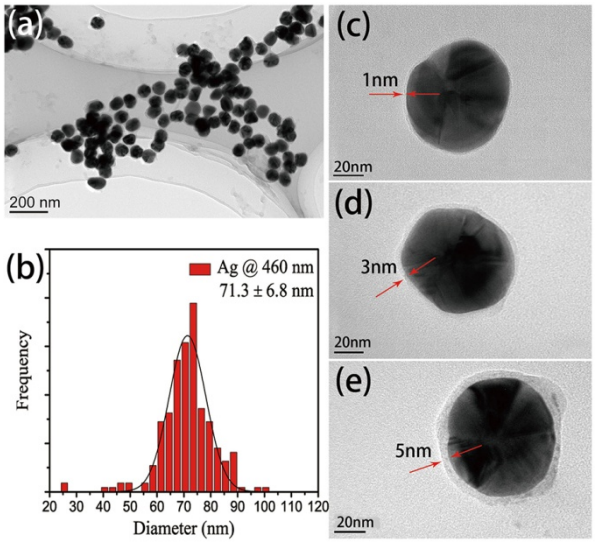

Fig. 1. (a) TEM image of Ag NPs. (b) NPs size distribution. (c), (d) and (e) are TEM images of Ag NPs with $(PAH/PSS)_n$/PAH layers (n = 0, 1, 2) with 1 nm, 3 nm, 5 nm shell thickness respectively.

Optics EXPRESS

Figure 1(a) shows a representative TEM image of silver NPs. Most of the NPs display a sub-circular shape with an average diameter of 71.3 ± 6.8 nm [Fig. 1(b)]. The silver NPs coated with ultrathin polyelectrolyte layers of different thicknesses are also identified by TEM [Figs. 1(c)–1(e)], which demonstrate that the shell thickness increases from 1 nm to 3nm and 5 nm with the increasing (PAH/PSS)n/PAH layers (n = 0, 1, 2).

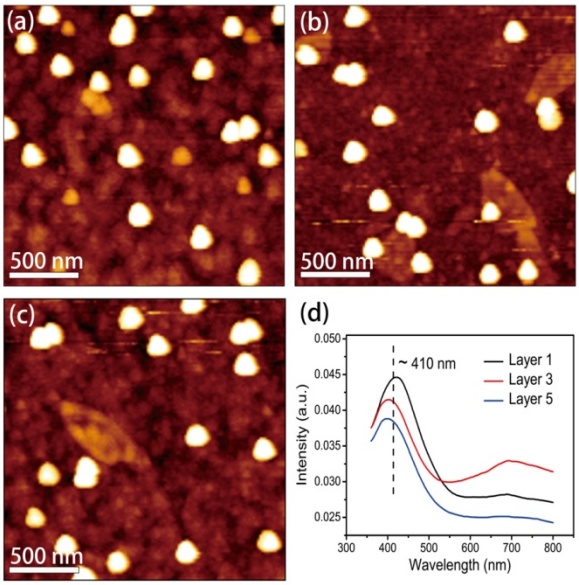

Fig. 2. (a), (b) and (c) are AFM images of TPP/Ag/$(PAH/PSS)_n$/PAH/Glass (n = 0, 1, 2). (d) UV-vis absorption spectra of the NPs with 1 nm (black), 3 nm (red), 5nm (blue) shell thickness on glass.

Typical AFM images for the Ag NPs with 1, 3, 5 polyelectrolyte layers spin-coated on the very smooth glass substrates (roughness below 0.8 nm) are shown in Figs. 2(a)–2(c), with similar distribution density. Figure 2(d) shows the absorption spectra of the silver-polymer core-shell NPs. It can be seen that the obvious absorption peaks for the three types of NPs appear at roughly the same position around 410 nm, which just coincides with the strong Soret absorption band (400 nm – 450 nm) of the porphyrin molecules [30]. Furthermore, the absorption intensity tends to decrease with the polymer thickness increasing, which is in good agreement with the previous literature [28].

For molecular coverage calibration, a representative STM topograph of submonolayer TPP on Au (111) at ~80 K are shown in Fig. 3(a). A number of molecular chains are observed to widely disperse on the Au (111) terraces with visible reconstruction ‘herringbone’ stripes. The chain configuration rises from intermolecular van der Waals forces and the weaker molecule-substrate interaction should be responsible for the diffusion and separation of the molecular chains. The existence of noisy regions in the STM image further proves the high mobility of the gas-phase molecules [25,31] even under liquid nitrogen temperature. Nominal equivalent TPP were evaporated to glass substrates under the same condition and molecules appear in the form of small clusters, sprinkled throughout the surface as imaged in AFM at room temperature [Fig. 3(b)]. Although elevated temperature resulted in stimulated surface migration and suppressed adhesion, the structure of TPP molecules on glass substrate is still less than a monolayer. Considering the molecular size (less than 2 nm) much smaller than the NPs (about 71 nm), the schematic of TPP/NPs/Glass structures is assumed in Fig. 3(c), submonolayer porphyrins attaching around the silver-polymer core-shell NPs.

Optics EXPRESS

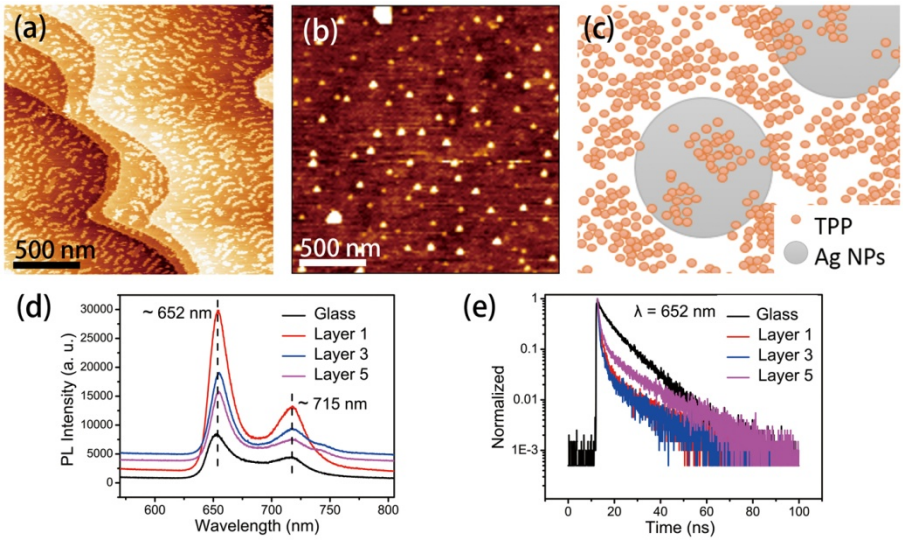

Fig. 3. (a) Typical STM image of TPP on Au (111) (200 × 200 nm^2, –2.6 V, 10 pA). (b) Typical AFM image of TPP on glass. (c) Schematic of Ag NPs coupled with submonolayer TPP molecules on glass. (d) and (e) are fluorescence spectra and dynamics of PL decay of the TPP/Glass and TPP/Ag/(PAH/PSS)$_n$/PAH/Glass, respectively.

Fluorescent spectra for TPP/NPs/Glass with different polyelectrolyte layers (1, 3, 5 layers) are plotted in Fig. 3(d), exhibiting typical band characteristics with two peaks at 652 nm and 715 nm, deriving from the porphyrin $Q_x(0,0)$ and $Q_x(0,1)$ transitions respectively, in line with the PL spectra of the TPP/Glass sample [the bottom curve of Fig. 3(d)]. Differing from the relatively unchanged peak positions, the luminescent intensity of TPP/NPs/Glass is found to be enhanced obviously comparing with that of TPP/Glass. From the luminescent enhancement factor (Table 1), we can see that the maximum enhancement factor about 2.3 can be obtained. Not only that, with the polyelectrolyte layers thickening, the declining tendency of radiative enhancement effect [Fig. 3(d)] is found to be well consonant with the downtrend of the NPs' absorption intensity [Fig. 2(d)]. By synthetically taking account for the NPs' absorption peak (~410 nm), porphyrins' absorption band (400 nm – 450 nm) and the laser wavelength (405 nm), the mechanism for the fluorescence enhancement may be attributed to the resonant excitation enhancement of TPP molecules in the plasmonic near field. The increment of the polymer shell thickness will reduce the resonant influence of the metal core on the fluorescent molecules, resulting in the suppression of the luminescent enhancement.

Table 1. Lifetimes and Enhancement Factor of the TPP/(PAH/PSS)$_n$/PAH and TPP/Glass Samples.

Sample	n	Enhancement factor	τ_1(ns), A_1	τ_2(ns), A_2	τ_3(ns), A_3
Glass	-	1	9.90, 79	2.65, 21	-
Layer 1	0	2.35	6.51, 31	0.70, 41	0.18, 28
Layer 3	1	1.23	6.85, 31	0.88, 23	0.16, 46
Layer 5	2	1.17	7.80, 50	1.35, 24	0.22, 26

In addition to the intensity change, we also observe that the full width at half maximum (FWHM) of the $Q_x(0,0)$ peak gradually becomes narrow with the shell thickening, from 23.6 nm for Ag/PAH to 19.8 nm for Ag/PAH/PSS/PAH and 18.0 nm for Ag/(PAH/PSS)$_2$/PAH. This dependence is closely related to the charge and energy transfer between the excited

Optics EXPRESS

molecules and the silver cores of NPs, which suggests the existence of potential interface quenching effect. The fluorescence decay curves as shown in Fig. 3(e) confirm our judgement, exhibiting faster decay processes (larger curve gradient) for TPP/NPs/Glass than that for TPP/Glass. Detailed lifetimes for the $Q_x(0,0)$ peak with related proportion are listed in Table 1. Two-exponential function can well fit the decay process of excited TPP molecules on pure glass, with a longer component τ_1 of 9.90 ns and a shorter component τ_2 of 2.65 ns. τ_1 can be assigned to the decay of monomer molecules while τ_2 is probably related to the excimers formation or molecular aggregation, which will lead to quenching effect by intermolecular π-π stacking interaction [32–34]. For the TPP/NPs/Glass samples, significant changes of decay processes occurr and a very fast nonradiative decay channel begins to emerge represented as the shortest lifetime τ_3 component of 0.16 ns – 0.22 ns. Considering TPP attaching on the silver-polymer core-shell NPs characterized as Fig. 3(c), nonradiative decay processes of molecular excited state should be much complicated, including several charge and energy transfer channels, such as the π-π stacking of neighboring molecules [34], surface interaction between molecules and polyelectrolyte layer [35], and molecules-metal coupling [34]. Similar to TPP/Glass sample, the τ_1 and τ_2 components can correspond to the decay of monomers and excimers or aggregates affected by intermolecular interaction via Förster resonance energy transfer mechanism respectively [34,35]. The emergence of the shortest lifetime τ_3 component in the TPP/NPs/Glass is mainly caused by the quenching of molecular fluorescence in the material system, which should be the result of the charge transfer via conductive polyelectrolyte layer [4] and non-radiative energy losses due to the absorption of silver NPs [3,5]. Moreover, the longer distances (thicker shells) will reduce the nonradiative energy losses, bringing out the slower decay rate (longer lifetime).

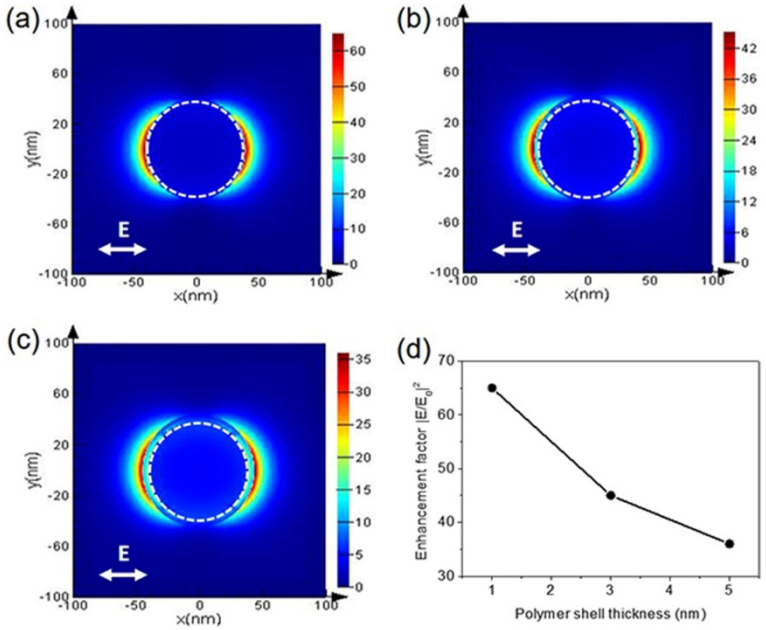

Fig. 4. Electric field enhancement ($|E/E_0|^2$) distribution images for the core-shell NPs at λ = 405 nm with the shell thickness 1 nm (a), 3 nm (b) and 5 nm (c), and the dash white circle represents Ag core. (d) the enhancement factor dependent on the polymer shell thickness.

For a radiative dipole (i.e., fluorescent dye molecules or quantum dots) under unsaturation excitation, its emission is a two-step process involving the excitation rate and the emission probability represented by the quantum yield. When coupling with plasmonic metallic NPs, both steps of the radiative dipole emission will be modified by surface plasmon of metallic NPs. During excitation, the incident light excites not only the dipole but also surface plasmon

Optics EXPRESS

of metallic NPs. The enhanced local near field produced by surface plasmon couples with the dipole and increases its excitation rate. And in the following emission process, the quantum yield is altered due to the presence of metallic NPs. In our case, Ag NPs with the diameter of ~71 nm show a plasmonic resonance at about 410 nm when deposited on glass substrate, which matches closely with the absorption band of TPP molecules and the excitation laser wavelength (405 nm). Therefore, the excitation enhancement plays a significant role in the fluorescent enhancement of TPP molecules when coupled with Ag NP-polymer core-shell nanostructures, and is proportional to the local near field enhancement $|E/E_0|^2$ of Ag NPs. To explain the observed distance-dependent fluorescence intensity of TPP molecules, the near filed distributions of Ag NPs with different polymer shell thickness were simulated using FDTD method. As shown in Figs. 4(a)–4(c), strong electric field enhancements ($|E/E_0|^2$) are observed around the shell surfaces of Ag NP-polymer core-shell nanostructures. The enhancement factor shows a nonlinear and rapid decrease with the increasing shell thickness [Fig. 4(d)], which is responsible for the decrease of the experimental fluorescence enhancement and absorption of Ag-polymer core-shell NPs with the shell thickness increasing. Obviously, the simulated near field enhancement factor is much larger than that obtained in experiment. This reason can be mainly ascribed to the fluorescence quenching effect induced by Ag NPs [3].

4. Conclusion

In summary, Ag-polymer core-shell NPs with the controlled shell thickness (1 nm – 5 nm) were synthesized. After submonolayer TPP molecules were deposited on the Ag-polymer core-shell NPs on glass substrates, the PL spectra and decay curves of the submonolayer TPP molecules were studied. The molecular fluorescence intensity is enhanced by the resonant excitation enhancement due to the good overlap between the plasmonic resonant peak of Ag-polymer core-shell NPs, the excitation laser wavelength and the absorption band of TPP molecules, and shows a decline as the increasing polymer shell thickness. The experimental enhancement factor is far below the theoretical one obtained by FDTD simulation mainly due to the quenching effect induced by the charge transfer and nonradiative energy transfer between excited molecules and the Ag-polymer core-shell NPs, which is confirmed by the fluorescence lifetime measurements.

Funding

National Key R&D Program of China (2017YFA0303403); the National Basic Research Program of China (2014CB921104); the National Nature Science Foundation of China (11674095, 11674099); Natural Science Foundation of Shanghai (16ZR1409400); Shuguang Program (15SG22); Shanghai International Cooperation Project (16520710600); 111 project (B12024).